Available online at www.sciencedirect.com

ScienceDirect

Ceramics International 41 (2015) 7197–7206

CERAMICS INTERNATIONAL

www.elsevier.com/locate/ceramint

Luminescent properties of $ZrO_2:Dy^{3+}$ and $ZrO_2:Dy^{3+}+Li^+$ films synthesized by an ultrasonic spray pyrolysis technique

A. Baéz-Rodríguez[a], O. Alvarez-Fragoso[b], M. García-Hipólito[b,*], J. Guzmán-Mendoza[c], C. Falcony[d]

[a]Postgrado en Ciencia e Ingeniería de Materiales, UNAM, Apartado Postal 70-360, Coyoacán 04510, México, D.F., Mexico

[b]Departamento de Materiales Metálicos y Cerámicos, Instituto de Investigaciones en Materiales, Universidad Nacional Autónoma de México, Apartado Postal 70-360, Coyoacán 04510 México, D.F., Mexico

[c]Centro de Investigación en Ciencia Aplicada y Tecnología Avanzada del Instituto Politécnico Nacional, Unidad Legaria, Calzada Legaria 694, Colonia Irrigación, Código Postal 11500, México, D.F., Mexico

[d]Departamento de Física, CINVESTAV-IPN, Apartado Postal 14-740, 07000 México, D.F., Mexico

Received 2 December 2014; received in revised form 22 January 2015; accepted 9 February 2015
Available online 14 February 2015

Abstract

$ZrO_2:Dy^{3+}$ and $ZrO_2:Dy^{3+}+xLi^+$ films were synthesized by an ultrasonic spray pyrolysis process. X-Ray Diffraction studies, as a function of the deposition temperature, indicate a meta-stable tetragonal crystal structure of the zirconia, as the substrate temperature was increased. Photoluminescence and cathodoluminescence characteristics of the films were studied as a function of deposition parameters such as the substrate temperature and the dysprosium and lithium concentrations. For an excitation wavelength of 286 nm, all the luminescent emission spectra show peaks located at 485, 584, 670 and 760 nm, which are the characteristic 4f→4f intra-transitions of Dy^{3+} ions and they correspond to electronic transitions $^4F_{9/2}\rightarrow{}^6H_{15/2}$, $^4F_{9/2}\rightarrow{}^6H_{13/2}$, $^4F_{9/2}\rightarrow{}^6H_{11/2}$ and $^4F_{9/2}\rightarrow{}^6H_{9/2}$, respectively. The lithium incorporation in the $ZrO_2:Dy^{3+}$ films produced an improvement in the intensity of the luminescent emission. As the deposition temperature is increased, a rise of the luminescence intensity is observed. Also, it is noted, a quenching of the luminescence, with increasing doping concentration. The elemental chemical composition of the layers, as determined by energy dispersive spectroscopy, is reported as well. In addition, the surface morphology characteristics of the films, as a function of the deposition temperature, are presented.

Keywords: A. Films; $ZrO_2:Dy^{3+}$; Warm-white luminescence; Spray pyrolysis; Li^+ codoping

1. Introduction

The ZrO_2 films possess a great scientific and technological importance due to their diverse advantages and applications, they have been deposited by several processes [1–3]; among them the Ultrasonic Spray Pyrolysis (USP) method is a relatively simple, economic and suitable for deposition over large areas. Diverse types of films have been deposited by this technique, some of them are: ZrO_2, HfO_2, Al_2O_3 and $ZnAl_2O_4$ [4–7].

Recently, substantial efforts have been focused on the synthesis of ceramic oxides optically activated with rare-earth ions, due to combination of the optical properties of rare-earth ions and the exceptional qualities of ceramic materials [8]. Among these ceramic materials, zirconia is a potential selection due to its superior properties such as chemical stability, high thermo-mechanical resistance, high thermal expansion coefficient, optical transparency, low thermal conductivity, ionic conductivity, catalytic properties, etc. [9–11]. The phonon energy in zirconia is low (about 470 cm^{-1}) which opens up the possibility of achieving higher luminescence efficiency of active ions incorporated into ZrO_2 matrix [12]. Some rare-earth ion-doped ZrO_2 materials can achieve special optical properties

*Corresponding author. Tel.: +52 55 56224598; fax: +52 55 56161371.
E-mail address: maga@unam.mx (M. García-Hipólito).

http://dx.doi.org/10.1016/j.ceramint.2015.02.048
0272-8842/

and a substantial amount of work has been reported such as ZrO_2:Eu [13], ZrO_2:Tb [14], ZrO_2:Tm [15], ZrO_2:Sm [16], ZrO_2:Er [17], etc. These doped materials may find applications in devices like active optical windows, optical amplifiers, lasers, color television screens and in the solution of some technological problems in the flat panel display industry.

Dy^{3+} is an ideal active ion for luminescent materials since it can produce white light even as a single ion. For this reason, studies on optical properties of Dy^{3+} doped materials have gained considerable importance. This ion has two intense emission bands in blue and yellow regions. The yellow emission is due to a hypersensitive transition which is strongly influenced by the crystal field of the matrix. Consequently, it is possible to adjust the intensity ratio of yellow to blue emission via choosing proper host lattices [18,19]. In addition of the white light applications, Dy^{3+} doped materials are widely studied for its optical amplification in the near infrared region and in the emission of laser radiation in the middle infrared region [20,21]. There are some investigations on Dy^{3+}-doped zirconia nanopowders [22–24] but no studies have been reported, to our knowledge, on the luminescent properties of Dy^{3+}-doped ZrO_2 films. The luminescent films are used in many important applications in the current technology. Compared to powder phosphors, luminescent films offer advantages such as: major thermal stability; good adherence to substrate; they do not present any degassing problems; have uniformed properties through the area covered; possess major resolution and contrast with minimal optical dispersion and all of this with the use of less material [25].

The present work reports the crystalline structure, the surface morphology, the chemical composition and the PL–CL properties of ZrO_2:Dy^{3+} and ZrO_2:$Dy^{3+}+xLi^{+}$ films deposited by means of the USP technique. The role that the substrate temperature and the activators concentration play on the above-mentioned properties is also reported.

2. Experimental procedure

The USP technique was used to deposit ZrO_2:Dy^{3+} and ZrO_2:$Dy^{3+}+x$Li films [26]. In this method an ultrasonic humidifier is used to produce a fine mist from the precursor solution. The mist is transported to a hot substrate located on a tin bath through a tubing setup using filtered air as a carrier gas, as a result a chemical reaction is carried out and a solid film is deposited on the substrate. The carrier gas was dry air with a flow rate of 10 liter/min. The precursor solutions were obtained from zirconium oxichloride ($ZrOCl_2 \cdot 8H_2O$, Aldrich Chemical Co.) and deionized water at 0.05 molar concentration. Doping with Dy^{3+} was achieved by adding $DyCl_3 \cdot 6H_2O$ (ALFA AESAR) in the range from 1 to 20 (1, 3, 5, 7, 10, 15 and 20) atomic percent (*a/o*) in relation to the Zr content in the start solution; the lithium source was $LiCl \cdot 6H_2O$ (ALFA AESAR). The substrate temperature (T_s) was varied in the range from 350 to 600 °C in steps of 50 °C. The substrates were either silicon single crystal or glass (Corning 7059) slides of about 1.5 cm^2. The deposition time was adjusted from 5 to 6 min to deposit films with approximately the same thickness. The thickness of the films studied was about 6 μm as measured by a Sloan Dektak IIA profilometer (within ± 0.3 μm). The crystalline structure of the films was analyzed by means of X-Ray Diffraction (XRD), using a Siemens D-5000 diffractometer with wavelength radiation of 1.5406 Å (Cu kα). The chemical composition of the films was measured using EDS (Energy Dispersive Spectroscopy) with a Jeol Scanning Electron Microscopy model JSM-7600F equipped with a Oxford INCA Energy+, Si–Li, X-ray detector. The surface morphology of the films studied was analyzed by means of the SEM (Scanning Electron Microscope) above-mentioned. The excitation (PLE) and the photoluminescence (PL) spectra were obtained by means of the spectrofluorometer fluoro-Max-P from Jobin Yvon Horiba. Cathodoluminescence (CL) measurements were performed in a stainless steel vacuum chamber with a cold cathode electron gun (Luminoscope, model ELM-2 MCA, RELION Co.). The films are positioned inside the vacuum chamber whose pressure is less than 10^{-3} Torr. The electron beam used to excite the samples is generated parallel to the surfaces of these films and, through a magnetic field; it is diverted 90° to incise perpendicular to the said surfaces. The visible radiation emitted from the samples is collected with an optic fiber and analyzed in the above-mentioned spectrofluorometer, where the luminescent spectra are recorded. The current of the electron beam was 0.03 mA and the diameter of this beam over the samples was 0.3 cm.

3. Results and discussion

In the Fig. 1, the results of XRD measurements on ZrO_2:Dy^{3+} (3 *a/o*) layers deposited at T_s from 400 °C to 550 °C are exhibited. The ZrO_2:Dy^{3+} coatings have poor crystallinity at low deposition temperatures (<400 °C), but for higher T_s, these films show well defined peaks which correspond to the zirconia tetragonal phase (according to 01-079-1764, ICSD 066783), indicating that samples are of single pure phase. Sharper diffraction peaks at high T_s indicate an increase in the

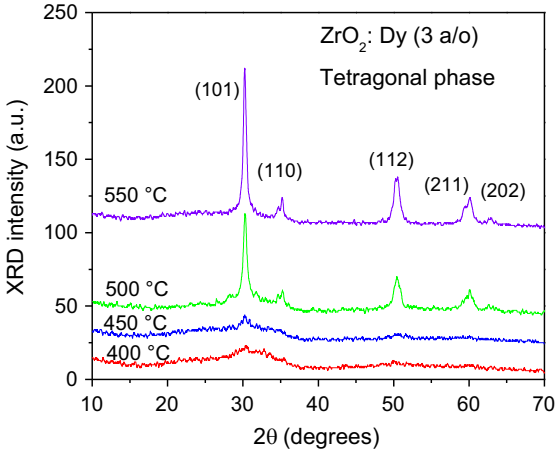

Fig. 1. XRD diffractograms for ZrO_2:Dy^{3+} (3 *a/o*) films grown at different T_s: 400 °C, 450 °C, 500 °C and 550 °C.

crystallite size as the deposition temperature raises. The peaks at 30.2°, 35.2°, 50.3°, 60.1° and 62.9° can be assigned to the crystallographic orientations (101), (110), (112), (211) and (202), respectively. The crystal size was estimated by means of the Scherrer formula using the most intense band (situated at $2\theta = 30.2°$); crystal size was determined to be 23 nm.

Tables 1 and 2 show the results of EDS measurements. Table 1 summarizes the relative atomic percentages of the oxygen, zirconium, dysprosium and chlorine incorporated into the films as a function of the content of the dysprosium chloride included in the spraying solution. A reduction of the relative content of zirconium and an increase in the relative contents of oxygen, chlorine and dysprosium are observed when the doping concentration is increased; the substrate temperature, in this case, was 550 °C. Table 2 shows similar results to that in Table 1 but now as a function of the substrate temperature, keeping fixed the doping concentration (dysprosium chloride 3 *a/o*) in the starting solution. It is observed that as the substrate temperature increases, the relative content of oxygen and zirconium is increased and a significant reduction in the relative contents of dysprosium and chlorine are also observed.

Fig. 2 shows SEM micrographs on the surface morphology of ZrO_2:Dy^{3+} coatings deposited at 400 °C (a), 450 °C (b), 500 °C (c), 550 °C (d), 600 °C (e) and a cross section for the film deposited at 550 °C (f). In general, rough but continuous films with good adherence to the substrate are observed. However, the surface morphology of the films depends on the substrate temperature; layers deposited at 400 °C present rough surfaces formed by an open network formed by thick "veins" or ramifications and some spherical particles. At 450 °C and 500 °C, the surface morphology evolves to compact structures formed by some veins and the growth of more spherical and pseudo-spherical particles on top of them. These characteristics are, very probably, obtained because at higher substrate temperature the deposited precursors have larger surface kinetic energy, which produces a more complete pyrolytic reaction of the reactant materials that result in a more compact film. The films deposited at 550 °C show a cavernous surface morphology free of veins formed mainly by clusters of pseudo-spherical particles. In the samples deposited at 600 °C, Fig. 2(e), the micrograph shows a surface morphology constituted by a great quantity of clusters formed by particles of pseudo-spherical shape. In this case, the morphology can be associated to the fact that at high temperatures, the precursor elements may react before they reach the substrate, generating a very fine powder of the final oxide. These clusters originate non-continuous films; it is possible to observe, in the bottom, parts of the substrate without material and some "disks" originated by aerosol drops that arrived as a liquid to the surface of the substrate. As a result, the "films" deposited at this substrate temperature (600 °C) do not have as good adherence to the substrate like those deposited at lower substrate temperature. Fig. 2(f) exhibits the cross section of a sample deposited at 550 °C, it is possible to observe a nodular growth rather than columnar one. The value of the thickness here observed is similar to the one measured by means of the profilometer.

Fig. 3 shows the PL excitation spectra for ZrO_2:Dy^{3+} (3 *a/o*) deposited at 550 °C. The emission wavelengths were fixed at 485 nm and 584 nm, which correspond to the most prominent bands observed in the emission spectrum (to see Fig. 4). It is possible to observe that the wide bands (from 225 nm to 310 nm) centered at 286 nm are practically identical when monitored at 485 or 584 nm. The spectra exhibit two distinct zones; the first zone is associated with above described broad band in the range of 225–310 nm. This strong broad band might be ascribed to the host absorption since the charge transfer band of the Dy–O is usually located at vacuum ultraviolet wavelengths [27]. The second zone involves excitation bands at longer wavelengths that are characteristic of f–f transitions originating from excited levels of the Dy^{3+} ions. These bands are located at 326, 355, 366 and 387 nm, which correspond to the transitions from the ground level: ($^6H_{15/2} \rightarrow {}^6P_{3/2}$), ($^6H_{15/2} \rightarrow {}^4F_{9/2}$), ($^6H_{15/2} \rightarrow {}^6P_{5/2}$) and ($^6H_{15/2} \rightarrow {}^4F_{7/2}$), respectively. The excitation located at 355 nm corresponds to the transition from the ground level $^6H_{15/2}$ to the hypersensitive level $^6P_{7/2}$, from where it relaxes nonradiatively to the $^4F_{9/2}$ metastable level. The excitation bands at 320–400 nm indicate that the ZrO_2:Dy^{3+} phosphor is suitable to be excited by near-UV LEDs. The general distribution of the observed peaks agrees with the reported structure of the spectra for ZrO_2:Dy^{3+} phosphors [28–30]. The inset of Fig. 3 exhibits the excitation and emission spectra for un-doped ZrO_2 films. The excitation

Table 1
Atomic percent content of the oxygen, zirconium, dysprosium and chlorine in the dysprosium-doped zirconium oxide films as measured by EDS for different $DyCl_3$ concentrations in the spraying solution. The substrate temperature was 550 °C.

$DyCl_3$ concentration in the spraying solution (*a/o*)	Oxygen (*a/o*)	Zirconium (*a/o*)	Dy (*a/o*)	Chlorine (*a/o*)
0	67.3	32.1	00.0	00.6
3	65.2	33.3	00.6	00.9
5	65.0	30.9	01.4	02.7
7	64.8	29.1	02.5	03.6
10	64.6	28.2	02.9	04.3
15	63.6	26.7	03.8	05.9
20	62.7	25.6	04.9	06.8

Table 2
Atomic percent content of the oxygen, zirconium, dysprosium and chlorine in the dysprosium-doped zirconium oxide films as determined by EDS for different substrate temperatures. In this case, the $DyCl_3$ concentration in the spraying solution was 3 *a/o*.

Substrate temperature (°C)	Oxygen (*a/o*)	Zirconium (*a/o*)	Dy (*a/o*)	Chlorine (*a/o*)
350	61.9	29.9	01.9	06.3
400	62.6	30.8	01.5	05.1
450	63.7	31.3	01.2	03.8
500	64.1	32.5	00.9	02.5
550	65.2	33.3	00.6	00.9

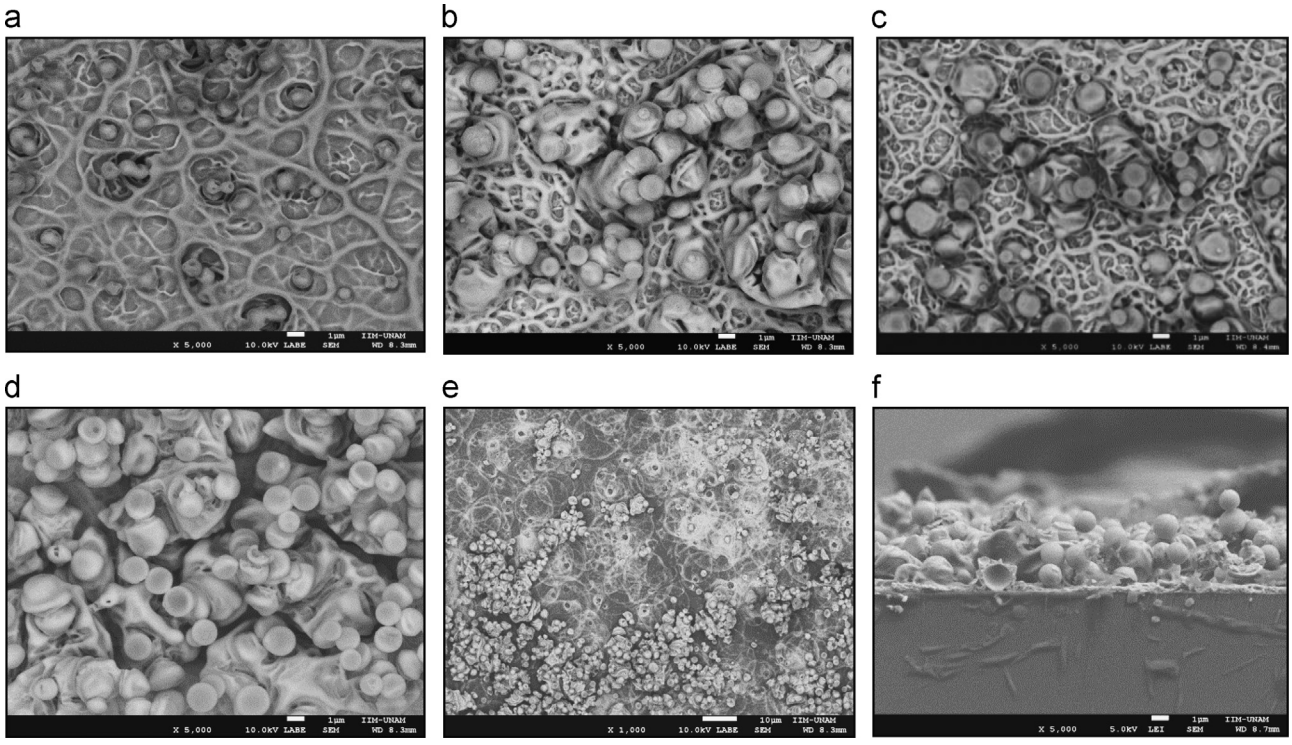

Fig. 2. SEM micrographs show the surface morphology of ZrO_2:Dy^{3+} (3 *a/o*) films as a function of the T_s: 400 °C (a), 450 °C (b), 500 °C (c), 550 °C (d), 600 °C (e) and 550 °C (cross section) (f).

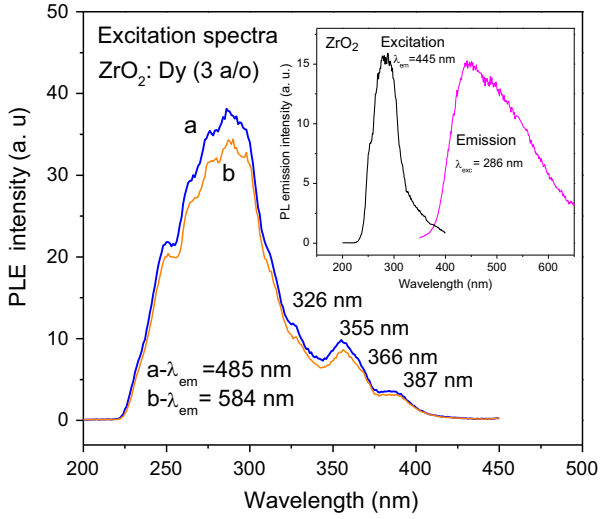

Fig. 3. Excitation spectra of ZrO_2:Dy^{3+} (3 *a/o*) films deposited at 550 °C. The excitation spectra were recorded with emission wavelengths fixed at 485 nm and 586 nm. The inset shows the PL excitation and emission spectra for pure ZrO_2 films.

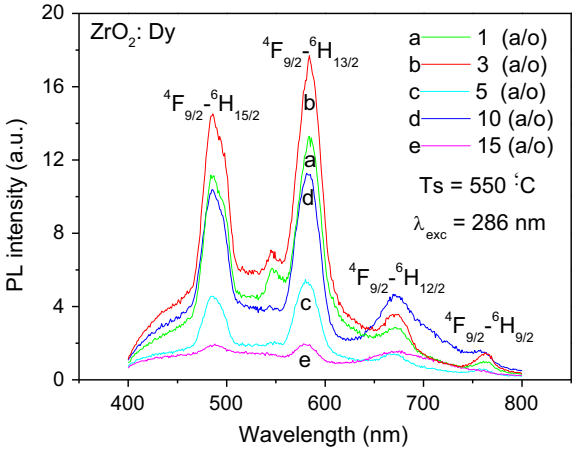

Fig. 4. PL emission spectra of ZrO_2:Dy^{3+} films deposited at 550 °C as a function of the doping concentration. The excitation wavelength was 286 nm.

spectrum presents a broad band centered at 286 nm which is assigned to the matrix absorption and coincides with that for the ZrO_2:Dy^{3+} films. The emission spectrum shows an asymmetrical broad band (400–650 nm) centered at 445 nm; a similar behavior is observed in ZrO_2 nanocrystalline powders [31]. This indicates that the PL emission observed in the ZrO_2:Dy^{3+} film is favored by the host lattice absorption. A 286 nm excitation wavelength was chosen to excite to the ZrO_2:Dy^{3+} films studied in this work.

PL emission spectra for ZrO_2:Dy^{3+} films are shown in the Fig. 4, as a function of the doping concentration in the spraying solution. In this case, the ZrO_2:Dy^{3+} films were synthesized at 550 °C and excited with a 286 nm wavelength. Here it is possible to distinguish four emission bands centered at 485 nm, 584 nm, 670 nm, 760 nm, which correspond, respectively, to the $^4F_{9/2} \rightarrow {}^6H_{15/2}$, $^4F_{9/2} \rightarrow {}^6H_{13/2}$, $^4F_{9/2} \rightarrow {}^6H_{11/2}$, and $^4F_{9/2} \rightarrow {}^6H_{9/2}$ characteristics transitions of the Dy^{3+} ions. The yellow band centered in 584 nm is the highest. Generally, the intensity of the PL emissions from

Dy^{3+} ions is notably disturbed by the surrounding symmetry of this ion in the host lattice. In the PL emission spectra it is possible to observe two main bands due to the Dy^{3+} ion; one in the blue region and the other in the yellow region of the electromagnetic spectrum. The blue emission is of magnetic nature and its intensity is practically independent of the matrix influence; on the other hand, the yellow emission is of electric nature and its intensity is very affected by the crystalline field of the host lattice. In both, the ZrO_2:Dy^{3+} and ZrO_2:Dy^{3+} + xLi^+ films the emission bands observed at 584 nm are stronger than the emission peaks located at 485 nm, which point out that Dy^{3+} ions occupy lower symmetry sites in this matrix [32]. The intensities of all the emission bands increase with the Dy^{3+} concentration until 3 *a/o* of $DyCl_3$ (in the spraying solution). Then, the intensity decreases due to the concentration quenching for higher values than 3 *a/o* of $DyCl_3$ (0.6 *a/o* of Dy as measured by EDS). As the Dy^{3+} concentration is increased, the average distance between Dy^{3+} ions will decrease; then cross relaxations between Dy^{3+} ions become more common; the following cross relaxations could be responsible for the nonradiative population decrease of $^4F_{9/2}$ multiplet: $^4F_{9/2}+{}^6H_{15/2} \rightarrow {}^6H_{9/2}({}^6F_{11/2})+{}^6F_{3/2}$, $^4F_{9/2}+{}^6H_{15/2} \rightarrow {}^6H_{5/2}+{}^6F_{7/2}$, and $^4F_{9/2}+{}^6H_{15/2} \rightarrow {}^6F_{1/2}+{}^6H_{9/2}({}^6F_{11/2})$. Due to the cross relaxations, Dy^{3+} ions at the $^4F_{9/2}$ multiplet can be de-excited to the $^6H_{9/2}(^6F_{11/2})$, $^6H_{5/2}$, or $^6F_{1/2}$ multiplet, in the mean-while Dy^{3+} ions at the ground state $^6H_{15/2}$ are excited to the $^6F_{3/2}$, $^6F_{7/2}$ or $^6H_{9/2}(^6F_{11/2})$ multiplet. Then, all the Dy^{3+} ions concerned in the cross relaxations relax to the ground state non-radiatively, as a consequence the emissions associated to the $^4F_{9/2}$ multiplet are quenched, in according to reference [33].

The ZrO_2:Dy^{3+} films have outstanding PL luminescent emissions, which can be appreciated at simple sight, with a normal room light, when they are excited with an ultraviolet lamp (254 nm). This indicates, at least qualitatively, the high intensity of the PL luminescent emissions.

In the Fig. 5 PL emission spectra for ZrO_2:Dy^{3+} (3 *a/o*) films are shown, as a function of the deposition temperature. Here, the ZrO_2:Dy^{3+} films were excited with a 286 nm wavelength and the doping concentration was 3 *a/o* of $DyCl_3$ in the spraying solution (0.6 *a/o* of Dy^{3+} as measured by EDS). Once again (like in the Fig. 4), it is possible to distinguish four emission bands centered at 485 nm, 584 nm, 670 nm, 760 nm, which correspond to the $^4F_{9/2} \rightarrow {}^6H_{15/2}$, $^4F_{9/2} \rightarrow {}^6H_{13/2}$, $^4F_{9/2} \rightarrow {}^6H_{11/2}$, and $^4F_{9/2} \rightarrow {}^6H_{9/2}$, respectively, typical transitions of the Dy^{3+} ions. The PL emissions increase in intensity as the substrate temperature is increased, probably due to an improved crystallization of the host material, as it is shown by XRD measurements, in this range of deposition temperatures and to the reduction of chlorine (and other undesired residuals) left into the films. Both effects will generate a better incorporation and distribution of the dysprosium ions into the host lattice, which will result in an increase of the PL emission as the deposition temperature is increased. It is possible to observe in this figure that the samples deposited at 550 °C have the highest emission intensity. According to the observed tendency, films deposited at substrate temperatures higher than 550 °C would have a more intense PL emission. The synthesized films at deposition temperatures greater than 550 °C (600 °C) did not have a total coverage on the substrate, show porosities and a poor adherence. Like mentioned before, this is probably due to the fact that at those temperatures the chemical reaction is performed in the vapor phase, before it gets to the substrate, generating a powdery and not continuous films. If it were possible to deposit continuous films, at 600 °C, with similar thickness to the one deposited at 550 °C, certainly this film would have the maximum emission intensity.

Fig. 6 shows PL emission spectra for ZrO_2:Dy^{3+} + xLi^+ films, as a function of the Li^+ ion concentration in the spraying solution. Here, the ZrO_2:Dy^{3+} + xLi^+ films were synthesized at 550 °C and excited with a 286 nm wavelength; the Dy doping concentration was fixed at 3 *a/o*. It is possible to distinguish four emission bands centered at 485 nm, 580 nm, 668 nm, and 755 nm, which correspond to the $^4F_{9/2} \rightarrow {}^6H_{15/2}$,

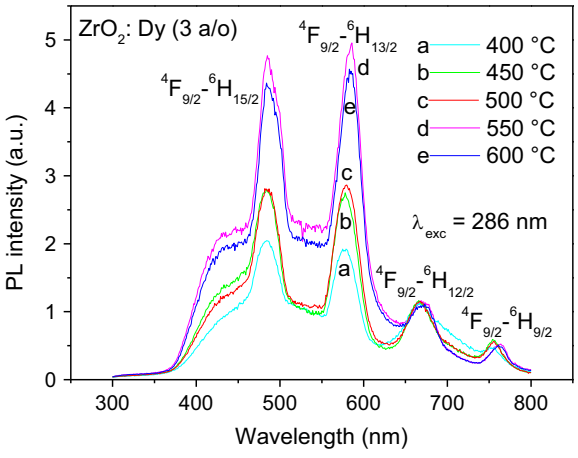

Fig. 5. PL emission spectra of ZrO_2:Dy^{3+} (3 *a/o*) films for different deposition temperatures. In this case, the excitation wavelength was 286 nm.

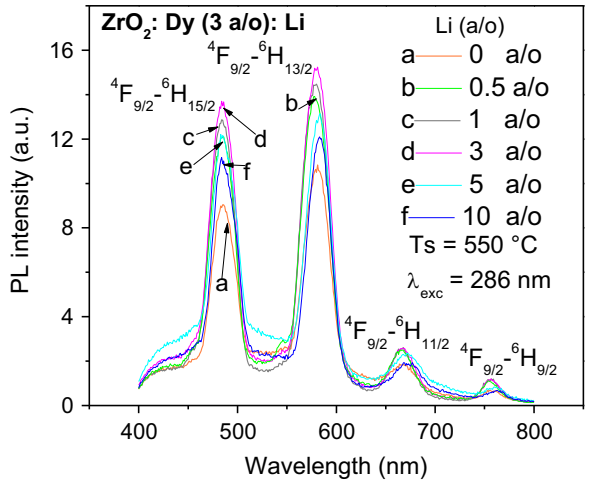

Fig. 6. PL emission spectra for ZrO_2:Dy^{3+} + xLi^+ films, as a function of Li^+ ions concentration in the spraying solution. These films were synthesized at 550 °C and excited with a 286 nm wavelength; the Dy^{3+} doping concentration was fixed at 3 *a/o*.

$^4F_{9/2} \rightarrow {}^6H_{13/2}$, $^4F_{9/2} \rightarrow {}^6H_{11/2}$, and $^4F_{9/2} \rightarrow {}^6H_{9/2}$ respectively transitions of the Dy^{3+} ions. The LiCl concentrations varied from 0.5 to 10 *a/o* (in the spraying solution). An improvement in the emission intensities with the lithium ions incorporation is clearly observed. Also, the PL spectra from ZrO_2:Dy^{3+} (3 *a/o*)+xLi^+ films show that Dy^{3+} emissions can be enhanced with the increasing codopant Li^+ content till $x=3$ *a/o*; the PL emission intensity decreases gradually when the Li^+ content exceeds $x=3$ *a/o*. However, notice that the samples with any quantity of Li^+ ions show a higher PL intensity than those without them. In this case, it is proposed that the Li^+ ions can act as co-activators and/or charge compensators and may assist for the energy transfer from the host lattice to the Dy^{3+} active center, resulting in a higher quantum yield. Acting as a co-activator and/or a charge compensator, Li^+ ions have been incorporated into diverse luminescent host lattices. There are many reports on the significant enhancement in emission intensity with Li^+ co-doping in different hosts [34,35]. Also, it is known that during the synthesis of these materials, different types of the structural defects are created; in the case Dy^{3+} ions incorporated into the ZrO_2 matrix, they enter in substitution of Zr ions, generating defects, mainly oxygen vacancies. When Li^+ ions are incorporated, they contribute to the neutralization of the electrical charge and prevent, in good measure, the formation of the oxygen vacancies; thus, the crystalline structure of the films improves. This fact contributes to carry out more affectively the energy transfer from the host lattice towards the Dy^{3+} ions, with which the intensity of the PL emission is notably improved. On the other hand, the presence of the Li^+ ions could favor changes of the environment of the Dy^{3+} ions and with this induce a more efficient light generation [36–38].

The Cathodoluminescence is a very important phenomenon that is used in devices based on cathode ray tubes, and it is often very useful in the characterization of luminescent materials [39]. CL emission spectra for ZrO_2:Dy^{3+} films are shown in Fig. 7 as a function of the doping concentration in the spraying solution. In this case, the ZrO_2:Dy^{3+} films were synthesized at 550 °C and measured under steady-state excitation; the applied electron accelerating voltage was 8 kV. As in the case of the PL, here it is possible to distinguish four emission bands centered at 485 nm, 584 nm, 670 nm, 760 nm, which correspond to the $^4F_{9/2} \rightarrow {}^6H_{15/2}$, $^4F_{9/2} \rightarrow {}^6H_{13/2}$, $^4F_{9/2} \rightarrow {}^6H_{11/2}$, and $^4F_{9/2} \rightarrow {}^6H_{9/2}$, respectively, transitions of the Dy^{3+} ions. The yellow band centered in 584 nm is once more the highest. Again, the intensities of all the emission bands increase with the Dy^{3+} concentration, the maximum emission intensity is obtained for 3 *a/o* of $DyCl_3$ (in the spraying solution). A concentration quenching of the CL emission is appreciated; the emission intensity decreases for higher values than 3 *a/o* of $DyCl_3$ (0.6 *a/o* of Dy as measured by EDS). When a material is optically activated with rare earths ions, as their concentration increases, the distance between these ions (in this case Dy^{3+} ions) is reduced causing energy transference between them, in way that said energy could get lost in the host lattice defects and so not contributes to the emission of visible light. As the thermal energy increases (on the substrate surface) it promotes a better dissociation of the precursor salts promoting a reduction of the residual impurities incorporated inside the films; this fact induces a better crystalline structure and a better distribution of the Dy^{3+} ions into the ZrO_2 matrix. As a consequence, an increase in the CL emission intensity is observed [40]. In this case, it is possible to distinguish a splitting of the blue band (for samples doped with 1, 3 and 5 *a/o* of $DyCl_3$) which is absent in the PL spectra. This splitting is probably associated to the influence of the asymmetric electric field produced by the crystalline environment (impurities or other defects) on the Dy^{3+} ions. This is known as the ligand-field effect [41]. It is not clear the nature of this result; more research is needed to elucidate this point.

Fig. 8 shows CL emission spectra of ZrO_2:Dy^{3+} films as a function of the deposition temperature. The electron accelerating voltage was 8 kV and the doping concentration in the spraying solution was fixed at 3 *a/o* of $DyCl_3$. These spectra show dominant bands centered at 485 nm, 586 nm and small peaks located at 673 nm and 760, which correspond, as in the

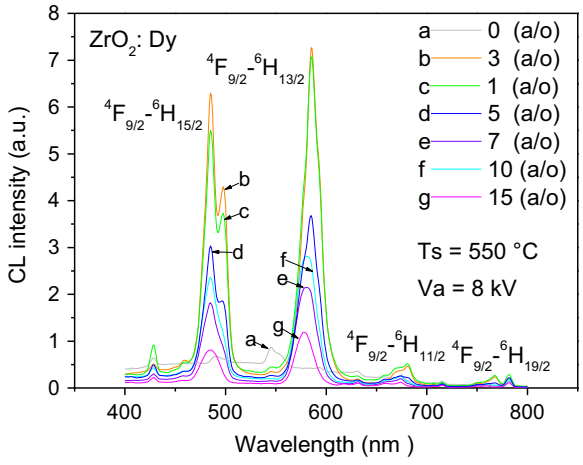

Fig. 7. CL emission spectra for ZrO_2:Dy^{3+} films as a function of the doping concentration in the spraying solution. ZrO_2:Dy^{3+} films were synthesized at 550 °C and the applied electron accelerating potential was 8 kV.

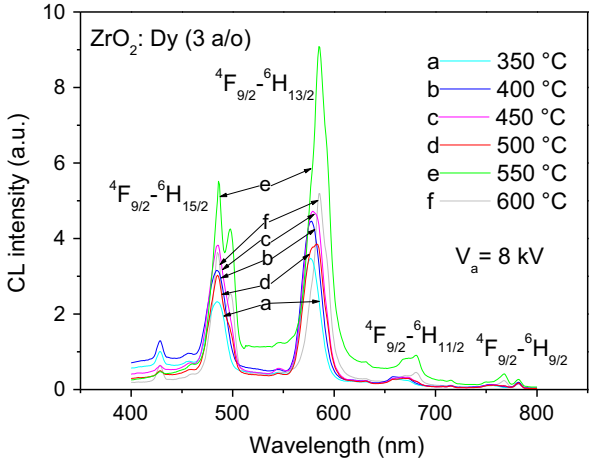

Fig. 8. CL emission spectra from ZrO_2:Dy^{3+} films, with variations on the deposition temperature. The electron accelerating voltage was 8 kV and the doping concentration in the spraying solution was fixed at 3 *a/o* of $DyCl_3$.

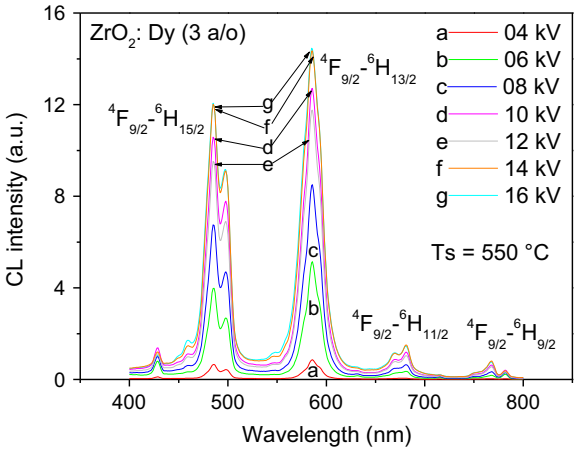

Fig. 9. CL emission spectra from ZrO_2:Dy^{3+} films, with variations of the applied electron accelerating voltages (4, 6, 8, 10, 12, 14 and 16 kV). The samples were deposited at 550 °C and the doping concentration was 3 *a/o*.

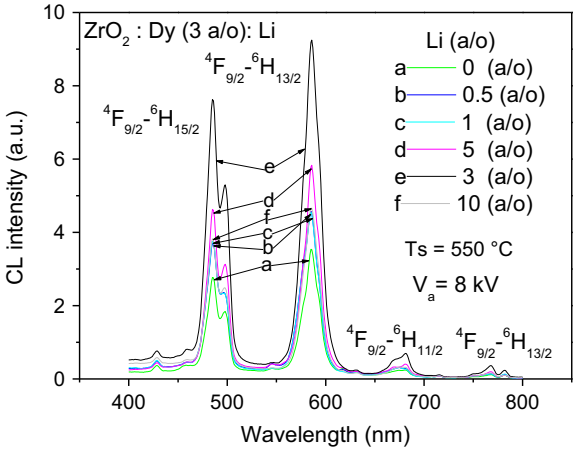

Fig. 10. CL emission spectra for ZrO_2:Dy^{3+} + xLi^{+} films, as a function of the Li^{+} ions concentration in the spraying solution. Films were synthesized at 550 °C, the electron accelerating voltage was 8 kV and the Dy^{3+} doping concentration was fixed at 3 *a/o*.

case of PL measurements, to the electronic transitions $^4F_{9/2} \rightarrow {}^6H_{15/2}$, $^4F_{9/2} \rightarrow {}^6H_{13/2}$, $^4F_{9/2} \rightarrow {}^6H_{11/2}$ and $^4F_{9/2}$–$^6H_{9/2}$ of the Dy^{+3} ions, respectively. Once again (as in PL measurements) the strongest emission corresponds to yellow $^4F_{9/2} \rightarrow {}^6H_{13/2}$ electronic transition. It is clear that the CL emission intensities rise with increasing substrate temperature (up to 550 °C), suggesting that a reduction of structural defects and the crystallite growth in the films favors the radiative recombination mechanisms. Also, the reduction of residual impurities (as chlorine, water, etc) incorporated into the crystallized samples produce a better incorporation and distribution of Dy^{3+} ions inside of host lattice, which could result in an growth of the CL emission intensities as the deposition temperature is raised.

Fig. 9 shows CL emission spectra from ZrO_2:Dy^{3+} films, with variations of the applied electron accelerating voltages (4, 6, 8, 10, 12, 14 and 16 kV). Here, the samples studied were deposited at 550 °C and the doping concentration was 3 *a/o*. The observed emission spectra consist of four bands characteristic of the Dy^{3+} ion (as in the case of the PL spectra), occurring within the 4f shell. Results show that the higher electron accelerating voltage produces the best emission intensity. In the CL phenomenon, the incident electrons penetrate a certain distance inside the material generating secondary electrons and hole–electron pairs. These incident and secondary electrons excite the Dy^{3+} ions to originate the visible light emission. When the electron accelerating voltage increases, a bigger volume of material is excited and there is a major generation of secondary electrons and hole–electron pairs, and so on. The hole–electron pairs recombination produce a greater amount of visible photons, which increases the intensity of the CL emissions. The visible light generation in the cathodoluminescence is an extremely complex process since during the stimulation with accelerated electrons X-rays are also produced, which excite to the Dy^{3+} ions generating even more visible light. Besides, the secondary electrons that where first created could in their own time produce even more electrons and hole–electron pairs, that contribute to a more efficient excitation and, in consequence, to produce a better CL emission intensity [42]. If it is observed through the window of the vacuum chamber, where the cathodoluminescence is performed, we can appreciate, at naked eye in normal room light, an intense yellowish-white light; this is a qualitative manifestation of the high intensity of the observed CL emissions.

Fig. 10 shows CL emission spectra for ZrO_2:Dy^{3+} + xLi^{+} films, as a function of the Li^{+} ions concentration in the spraying solution. Here, the ZrO_2:Dy^{3+} + xLi^{+} films were synthesized at 550 °C, the electron accelerating voltage was 8 kV and the Dy doping concentration was fixed at 3 *a/o*. Results in this figure are very similar to those of the Fig. 6. In this case, it is significant that both blue and yellow emission bands of Dy^{3+} ions enhance with the increasing content of Li^{+} till $x=3$ *a/o*, the emission intensity begin to decrease when the Li^{+} content exceeds this critical value. The emission intensity of the strongest band (586 nm) with the $x=3$ *a/o* (Li^{+}) is observed about three times higher than that of the film without codopant Li^{+}. The enhanced luminescence of the studied ZrO_2:Dy^{3+} + xLi^{+} films, may be associated with the charge balance principle of Li^{+} ions.

The ZrO_2:Dy^{3+} films show intense PL emissions in blue (485 nm) and yellow (584 nm) zones and the appropriate combination of blue and yellow light can produce white light emission. In order to find out color coordinates of these films, the emission spectra (as a function of the doping concentration in the spraying solution and deposited at 550 °C) have been analyzed in the frame work of CIE (Commission Internationale de l'Eclairage) 1931 chromaticity coordinates diagram. The calculated chromaticity coordinates of the films are shown in Fig. 11. From the figure it is found that color coordinates of all the samples fall in the white light region. Hence these samples can be used as white light emitting materials. The CIE coordinates under excitation at 286 nm are: (0.3647, 0.4147), (0.3597, 0.4059), (0.3531, 0.3956), (0.3479, 0.3883) and (0.3308, 0.3761) for 1, 3, 5, 10, and 15 Dy *a/o*, respectively. It can be observed that, as the concentration of Dy^{3+}

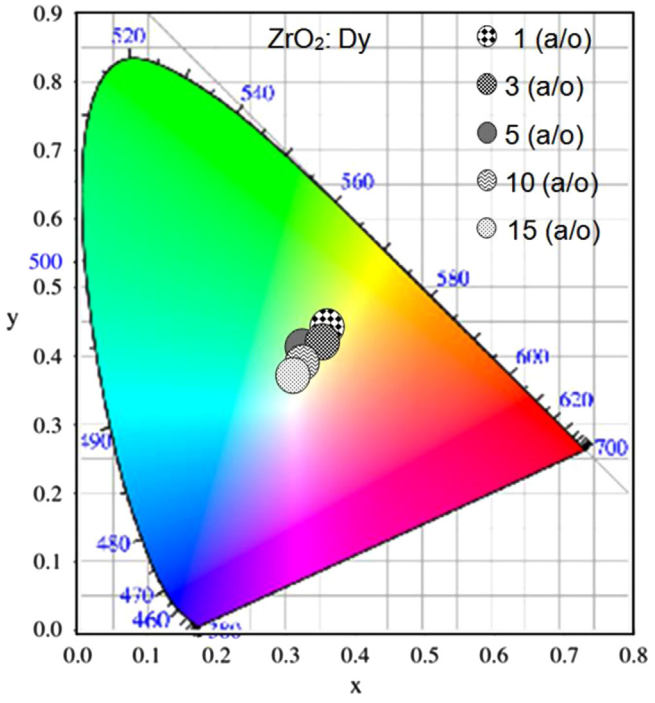

Fig. 11. CIE chromaticity diagram for ZrO_2:Dy^{3+} films as a function of the doping concentration. The excitation wavelength was 286 nm. The films were deposited at 550 °C.

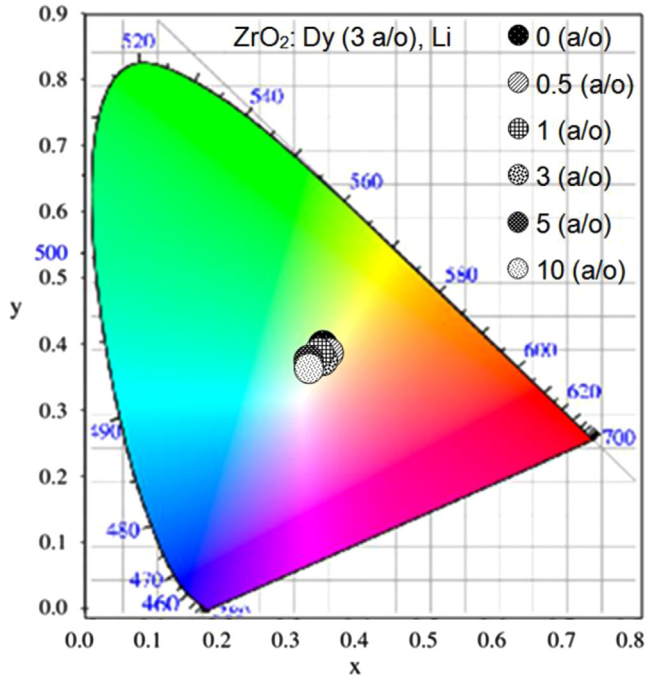

Fig. 12. CIE chromaticity diagram for ZrO_2:Dy^{3+} + xLi^{+} films as a function of the Li^{+} doping concentration. The excitation wavelength was 286 nm. The films were deposited at 550 °C and the Dy^{3+} doping concentration was fixed at 3 *a/o*. (For interpretation of the references to color in this figure, the reader is referred to the web version of this article.)

increases, the color of the films is close to the equal energy white light point (0.3333, 0.3333).

Fig. 12 shows the CIE chromaticity coordinates for ZrO_2: Dy^{3+} + xLi^{+} films, as a function of the Li^{+} ions concentration in the spraying solution. ZrO_2:Dy^{3+} + xLi^{+} films were synthesized at 550 °C and excited with a 286 nm wavelength; the Dy^{3+} doping concentration was fixed at 3 *a/o*. Based on the standard CIE coordinate-color graph, it is possible to observe that ZrO_2: Dy^{3+} + xLi^{+} films can emit warm-white light with CIE coordinates (0.3608, 0.4002), (0.3548, 0.3923), (0.3560, 0.3859), (0.3559, 0.3846), (0.3406, 0.3707) and (0.3475, 0.3609) corresponding to x=0, 0.5, 1, 3, 5 and 10 (Li^{+} *a/o*), respectively. It is observed that, as the concentration of Li^{+} ions increases, they come closer to the white perfect area.

4. Conclusions

In this contribution, the PL and CL emissions (yellowish-white) from ZrO_2:Dy^{3+} and ZrO_2:Dy^{3+} + xLi^{+} films, synthesized by the ultrasonic spray pyrolysis process, were studied. The XRD measurements on these films showed that its crystallinity depends on the deposition temperature; at low temperatures they are in the non-crystalline state and when increasing the deposition temperature they changed to metastable polycrystalline tetragonal phase of the zirconia. The surface morphology of the films was also dependent on the deposition temperature; SEM micrographs showed that these films are rough, continuous and denser as the substrate temperature is increased. These films show a nodular and uniform growth on whole area of substrate except for films deposited at 600 °C. The films showed high deposition rate up to 1 μm per minute with an average thickness of 6 microns. The estimated grain size was 23 nm. It was determined that substrate temperature for the samples with maximum PL and CL emission intensities was 550 °C. The excitation spectra showed wide bands (from 225 nm to 310 nm) centered at 286 nm practically identical when monitored at 485 or 584 nm. The peaks observed below 300 nm are usually related to 4f–5d transitions or Dy–O charge transfer bands and above 300 nm they are related to 4f–4f transitions of the Dy^{3+} ions. Experimental results reveal that the luminescence (PL and CL) was affected by both the deposition temperature and the Dy^{3+} concentration in the ZrO_2 films. The observed luminescence emissions from ZrO_2:Dy^{3+} films are host sensitized and are typical of the Dy^{3+} electronic transitions. All PL and CL spectra showed four emission bands centered at 485 nm, 584 nm, 670 nm, 760 nm, which correspond, respectively, to the $^4F_{9/2} \rightarrow {}^6H_{15/2}$, $^4F_{9/2} \rightarrow {}^6H_{13/2}$, $^4F_{9/2} \rightarrow {}^6H_{11/2}$, and $^4F_{9/2} \rightarrow {}^6H_{9/2}$ transitions of the Dy^{3+} ions. The PL and CL intensity emissions are incremented as the substrate temperature increases. A concentration quenching of the luminescence emission is observed above the optimum concentration of 3 *a/o* (0.6 *a/o* of Dy^{3+} as measured by EDS). The PL and CL results of ZrO_2:Dy^{3+} and ZrO_2:Dy^{3+} + xLi films showed that the strongest luminescence corresponds to 0.6 *a/o* of Dy^{3+} and its emission intensity can be further enhanced about three times by codoping with 3 *a/o* of LiCl in the spraying solution. The reason is that Li^{+} ions may act as a promoter for better crystallization and as charge compensator. The CIE color coordinates of the studied films were found within the warm-white light emission region. The spectral characteristics of

these ZrO_2:Dy^{3+} and ZrO_2:Dy^{3+} + xLi films make it a promising candidate for application on optical devices and solid-state lighting for general illumination purposes, especially for white lighting applications.

A great advantage of the materials studied in this work is that the deposition temperature (400–550 °C, for films) is much lower than that of the traditional solid-state reaction method and other synthesis methods (800–1200 °C, for powders). These luminescent films could be integrated to optoelectronic devices, such as electroluminescent multilayer type MISIM (Metal-Insulator-Semiconductor-Insulator-Metal) for images in flat panel displays.

Finally, from the obtained results, it is possible to conclude that ZrO_2 is an appropriate host lattice to the Dy^{3+} ions in order to generate intense luminescent emissions, and that the simple and economical ultrasonic spray pyrolysis technique is very convenient and adequate to deposit films with remarkable qualities.

Acknowledgments

The authors would like to thank to Professor Prashant Patil for CIE program, to Adriana Tejeda for XRD measurements, Omar Novelo for EDS and SEM measurements and to M. Guerrero, Z. Rivera, H. Zarco, C. Flores and R. Reyes for their technical support.

References

[1] D. Perednis, O. Wilhelm, S.E. Pratsinis, L.J. Gauckler, Morphology and deposition of thin yttria-stabilized zirconia films using spray pyrolysis, Thin Solid Films 474 (2005) 84–95.

[2] D. Pamu, K. Sudheendran, M. Ghanashyam Krishna, K.C. James Raju, Anil K. Bhatnagar, Ambient temperature stabilization of crystalline zirconia thin films deposited by direct current magnetron sputtering, Thin Solid Films 517 (2009) 1587–1591.

[3] Francisco Trivinho-Strixino, Francisco E.G. Guimarães, Ernesto C. Pereira, Zirconium oxide anodic films: optical and structural properties, Chem. Phys. Lett. 461 (2008) 82–86.

[4] F. Ramos-Brito, M. García-Hipólito, C. Alejo-Armenta, O. Alvarez-Fragoso, C. Falcony, Characterization of luminescent praseodymium-doped ZrO_2 coatings deposited by ultrasonic spray pyrolysis technique, J. Phys. D: Appl. Phys. 40 (2007) 6718–6724.

[5] J. Guzmán-Mendoza, M.A. Aguilar-Frutis, G. Alarcón-Flores, M. García-Hipólito, A. Maciel-Cerda, J. Azorín-Nieto, T. Rivera-Montalvo, C. Falcony, Synthesis and characterization of hafnium oxide films for thermo and photoluminescence applications, Appl. Radiat. Isot. 68 (2010) 696–699.

[6] S. Carmona-Téllez, C. Falcony, M. Aguilar -Frutis, G. Alarcón-Flores, M. García-Hipólito, R. Martínez- Martínez, White light emitting transparent doublé layer stack of Al_2O_3:Eu^{3+}, Tb^{3+}, and Ce^{3+} films deposited by spray pyrolysis, ECS J. Solid State Sci. Technol. 2 (2013) R111–R115.

[7] M. García-Hipólito, J. Guzmán-Mendoza, E. Martínez, O. Alvarez-Fregoso, C. Falcony, Growth and cathodoluminescent characteristics of blue emitting cerium-doped zinc aluminate layers synthesized by spray pyrolysis technique, Phys. Status Solidi (a) 201 (2004) 1510–1517.

[8] A. Gedanken, R. Reisfeld, E. Sominski, O. Palchik, Yu Kiltypin, G. Panczer, M. Gaft, H. Minti, Sonochemical preparation and characterization of europium oxide doped in and coated on ZrO_2 and yttrium-stabilized zirconium (YSZ), J. Phys. Chem. B 204 (2000) 7057–7065.

[9] C.M. Leroy, T. Cardinal, V. Jubera, C. Aymonier, M. Treguer-Delapierre, C. Boissière, D. Grosso, C. Sanchez, B. Viana, F. Pellé, Luminescence properties of ZrO_2 mesoporous thin films doped with Eu^{3+} and Ag_n, Microporous Mesoporous Mater. 170 (2013) 123–130.

[10] A.S. Kao, G.L. Gorman, Modification of zirconia film properties by low-energy ion bombardment during reactive ion-beam deposition, J. Appl. Phys. 67 (1990) 3826–3834.

[11] K. An, K.S. Ravichandran, R.E. Dutton, S.L. Semiatin, Microstructure, texture, and thermal conductivity of single-layer and multilayer thermal barrier coatings of Y_2O_3-stabilized ZrO_2 and Al_2O_3 made by physical vapor deposition, J. Am. Ceram. Soc. 82 (1999) 399–406.

[12] E. De la Rosa, L.A. Diaz-Torres, P. Salas, R.A. Rodríguez, Visible light emission under UV and IR excitation of rare earth doped ZrO_2 nanophosphor, Opt. Mater. 27 (2005) 1320–1325.

[13] M. García-Hipólito, E. Martínez, O. Álvarez-Fregoso, C. Falcony, M.A. Aguilar-Frutis, Preparation and characterization of Eu doped zirconia luminescent films synthesized by pyrosol technique, J. Mater. Sci. Lett. 20 (2001) 1799–1801.

[14] E. Pereyra-Perea, M.R. Estrada-Yáñez, M. García, Preliminary studies on luminescent terbium doped ZrO_2 thin films prepared by sol-gel process, J. Phys. D: Appl. Phys. 31 (1998) L7–L10.

[15] Hongwu Zhang, Xiaoyan Fu, Shuyun Niu, Qin Xin, Blue emission of ZrO_2:Tm nanocrystals with different crystal structure under UV excitation, J. Non-Cryst. Solids 354 (2008) 1559–1563.

[16] S. Lange, I. Sildos, M. Hartmanova, J. Aarik, V. Kiisk, Luminescence properties of Sm^{3+}-doped polycrystalline ZrO_2, J. Non-Cryst. Solids 354 (2008) 4380–4382.

[17] A. Martínez-Hernández, J. Guzmán-Mendoza, T. Rivera-Montalvo, D. Sánchez-Guzmán, J.C. Guzmán-Olguín, M. García-Hipólito, C. Falcony, Synthesis and cathodoluminescence characterization of ZrO_2:Er^{3+} films, J. Lumin. 153 (2014) 140–143.

[18] Ganngam Phaomei, W. Rameshwor Singh, R.S. Ningthoujam, Solvent effect in monoclinic to hexagonal phase transformation in $LaPO_4$:RE (RE = Dy^{3+}, Sm^{3+}) nanoparticles: photoluminescence study, J. Lumin. 131 (2011) 1164–1171.

[19] N. Shanta Singh, R.S. Ningthoujam, Ganngam Phaomei, S. Dorendrajit Singh, A. Vinu, R.K. Vatsa, Re-dispersion and film formation of $GdVO_4$:Ln^{3+} (Ln^{3+} = Dy^{3+}, Eu^{3+}, Sm^{3+}, Tm^{3+}) nanoparticles: particle size and luminescence studies, Dalton Trans. 41 (2012) 4404.

[20] B. Shanmugavelu, V.V. Ravi Kanth Kumar, Luminescence studies of Dy^{3+} doped bismuth zinc borate glasses, J. Lumin. 146 (2014) 358–363.

[21] G.Q. Wang, X.H. Gong, Y.J. Chen, J.H. Huang, Y.F. Lin, Z.D. Luo, Y.D. Huang, Synthesis and photoluminescence properties of near-UV pumped yellow-emitting $Li_3Ba_2La_3(WO_4)_8$:Dy^{3+} phosphors, Opt. Mater. 36 (2014) 1255–1259.

[22] Feng Gu, Shu Fen Wang, Meng Kai Lu, Guang Jun Zhou, Su Wen Liu, Dong Xu, Duo Rong Yuan, Effect of Dy^{3+} doping and calcinations on the luminescence of ZrO_2 nanoparticles, Chem. Phys. Lett. 380 (2003) 185–189.

[23] L.A. Diaz-Torres, E. De la Rosa, P. Salas, V.H. Romero, C. Angeles-Chávez, Efficient photoluminescence of Dy^{3+} at low concentrations in nanocrystalline ZrO_2, J. Solid State Chem. 181 (2008) 75–80.

[24] Xiaoyan Fu, Shuyun Niu, Hongwu Zhang, Qin Xin, Photoluminescence of Dy^{3+} ions in yttrium-stabilized zirconium oxide with different phases, Mater. Sci. Eng. B 129 (2006) 14–17.

[25] G.A. Hirata, J. McKittrick, M. Avalos-Borja, J.M. Siqueiros, D. Devlin, Physical properties of Y_2O_3:Eu luminescent films grown by MOCVD and laser ablation, Appl. Surf. Sci. 113/114 (1997) 509–514.

[26] T.T. Koda, M.J. Hampden-Smith, in: Aerosol Processing of Materials, Wiley-VCH, New York, 1999.

[27] Xiaoyan Fu, Shuyun Niu, Hongwu Zhang, Qin Xin, Photoluminescence of Dy^{3+} ions in yttrium-stabilized zirconium oxide with different phases, Mater. Sci. Eng. B 129 (2006) 14–17.

[28] K. Lemanski, P.J. Deren, Luminescent properties of dysprosium (III) ions in $LaAlO_3$ nanocrystallites, J. Rare Earths 29 (2011) 1195–1197.

[29] L. Robindro Singh, R.S. Ningthoujam, N. Shanta Singh, S. Dorendrajit Singh, Probing Dy^{3+} ions on the surface of nanocrystalline YVO_4: luminescence study, Opt. Mater. 32 (2009) 286–292.

[30] L. Robindro Singh, R.S. Ningthoujam, Critical view on energy transfer, site symmetry, improvement in luminescence of Eu^{3+}, Dy^{3+} doped YVO_4 by core-shell formation, J. Appl. Phys. 107 (2010) 104304.

[31] S. Dhiren Meetei, S. Dorendrajit Singh, N. Shanta Singh, V. Sudarsan, R.S. Ningthoujam, M. Tyagi, S.C. Gadkari, R. Tewari, R.K. Vatsa, Crystal structure and photoluminescence correlations in white emitting nanocrystalline ZrO_2:Eu^{3+} phosphor: effect of doping and annealing, J. Lumin. 132 (2012) 537–544.

[32] M. Yu, J. Lin, Z. Wang, J. Fu, S. Wang, H.J. Zhang, Y.C. Han, Fabrication, patterning, and optical properties of nanocrystalline YVO_4:A (A = Eu^{3+}, Dy^{3+}, Sm^{3+}, Er^{3+}) phosphor films via sol−gel soft lithography, Chem. Mater. 14 (2002) 2224–2231.

[33] D. Parisi, A. Toncelli, M. Tonelli, E. Cavalli, E. Bovero, A. Belletti, Optical spectroscopy of BaY_2F_8:Dy^{3+}, J. Phys. Condens. Matter 17 (2005) 2783–2790.

[34] G. Rajan, K.G. Gopchandran, Effect of substrates on the photoemission properties of Li doped Gd_2O_3:Eu^{3+} nanocrystalline films, Opt. Mater. 33 (2011) 494–500.

[35] K.W. Chae, T.R. Park, C. Cheon, N.I. Cho, J.S. Kim, The enhancement of luminescence in co-doped cubic Eu_2O_3 using Li^+ and Al^{3+} ions, J. Lumin. 131 (2011) 2597–2605.

[36] Qingqing Du, Guangjun Zhou, Juan Zhou, Xiao Jia, Haifeng Zhou, Enhanced luminescence of novel $Y_2Zr_2O_7$: Dy^{3+} phosphors by Li^+ co-doping, J. Alloy. Compd. 552 (2013) 152–156.

[37] A.K. Parchur, A.I. Prasad, S.B. Rai, R.S. Ningthoujam, Improvement of blue, white and NIR emissions in YPO_4:Dy^{3+} nanoparticles on co-doping of Li+ ions, Dalton Trans. 41 (2012) 13810–13814.

[38] Xin-Yuan Sun, Jun-Cheng Zhang, Xin-Gen Liu, Liang-Wu Lin, Enhanced luminescence of novel $Ca_3B_2O_6$:Dy^{3+} phosphors by Li^+-codoping for LED applications, Ceram. Int. 38 (2012) 1065–1070.

[39] B.G. Yacobi, D.B. Holt, in: Cathodoluminescence Microscopy of Inorganic Solids, Plenum, New York, 1990.

[40] T. Hase, T. Kano, E. Nakasawa, H. Yamamoto, Phosphors materials for cathode-ray tubes, Advances in Electronics and Electron Physics, Vol. 79, Academic Press, London, 1990, p. 271.

[41] J.G.C. Bunzli, G.R. Choppin, in: Lanthanide Probes in Life, Chemical and Earth Sciences; Theory and Practices, Elsevier, Amsterdam, 1989.

[42] L. Ozawa, in: Cathodoluminescence: Theory and Applications, Kodansha-VCH Verlag, Germany, 1990, p. 9.